Journal of Power Sources 262 (2014) 494–500

Contents lists available at ScienceDirect

Journal of Power Sources

journal homepage: www.elsevier.com/locate/jpowsour

Integration of MnO_2 thin film and carbon nanotubes to three-dimensional carbon microelectrodes for electrochemical microcapacitors

Shulan Jiang [a], Tielin Shi [a,b], Dan Liu [a], Hu Long [a], Shuang Xi [a], Fengshun Wu [b], Xiaoping Li [b], Qi Xia [a], Zirong Tang [a,b,*]

[a] State Key Laboratory of Digital Manufacturing Equipment and Technology, Huazhong University of Science and Technology, Wuhan 430074, China
[b] Wuhan National Laboratory for Optoelectronics, Wuhan 430074, China

HIGHLIGHTS

- 3D Carbon microelectrode integrated with CNTs and MnO_2 film is presented.
- An optimized process is developed for large-scale production of hybrid electrodes.
- The hybrid electrode shows greatly increased specific geometric capacitance.
- The microelectrode array is suitable for on-chip energy storage.

ARTICLE INFO

Article history:
Received 18 September 2013
Received in revised form
4 November 2013
Accepted 2 December 2013
Available online 11 December 2013

Keywords:
3D hybrid microelectrode
On-chip microcapacitor
Carbon nanotube
Manganese dioxide
Large-scale manufacturing

ABSTRACT

Large-scale three-dimensional (3D) hybrid microelectrodes have been fabricated through modified carbon microelectromechanical systems (Carbon-MEMS) process and electrochemical deposition method. Greatly improved electrochemical performance has been shown for the 3D photoresist-derived carbon microelectrodes with the integration of carbon nanotubes (CNTs) and manganese dioxide (MnO_2). The electrochemical measurements of the microelectrodes indicate that the specific geometric capacitance can reach up to 238 mF cm^{-2} at the current density of 0.5 mA cm^{-2}. The capacitance loss is less than 18.2% of the original value after 6000 charge–discharge cycles. This study shows that stacking of MnO_2 film and integrating of CNTs to the 3D glassy carbon microelectrodes have great potential for on-chip microcapacitors as energy storage devices, and the presented approach is promising for large-scale and low-cost manufacturing.

1. Introduction

Due to ever-increasing environmental pollution and depletion of fossil fuels, development of eco-friendly high-performance energy storage and energy conversion devices has become a hot topic [1,2]. In recent years, miniaturized on-chip power sources are in great need owing to the spring up of miniaturized electronic devices. Different types of energy storing devices such as lithium-ion batteries, lead-acid batteries, and electrochemical capacitors have been made considerable progress [3]. Among them, electrochemical capacitors, also called supercapacitors, have attracted much attention due to their fast charge-discharge process, high power density, and reliable cycling life [1,4–7]. In addition, supercapacitors can be coupled with energy harvesting devices and micro-batteries to improve cycle life time [8] and provide sufficient peak power as required.

To develop high-performance supercapacitors with large specific capacitances and high energy/power densities, many kinds of capacitive materials have been investigated. Carbon materials (e.g., graphene [9] and CNTs [10,11]) are extensively studied because of their advantages of high surface area, high electrical conductivity, and environmental friendliness. Transition metal oxides such as MnO_2 [12–16], ruthenium dioxide (RuO_2) [17], and conductive polymers [18] are also promising supercapacitor materials owing to their high specific capacitance [13,18,19]. MnO_2 is one of the most promising pseudocapacitive materials due to its high theoretical

* Corresponding author. 1037 Luoyu Road, Wuhan 430074, China. Tel.: +86 27 87792241; fax: +86 27 87792413.
E-mail address: zirong@hust.edu.cn (Z. Tang).

0378-7753/$ – see front matter © 2013 Elsevier B.V. All rights reserved.
http://dx.doi.org/10.1016/j.jpowsour.2013.12.009

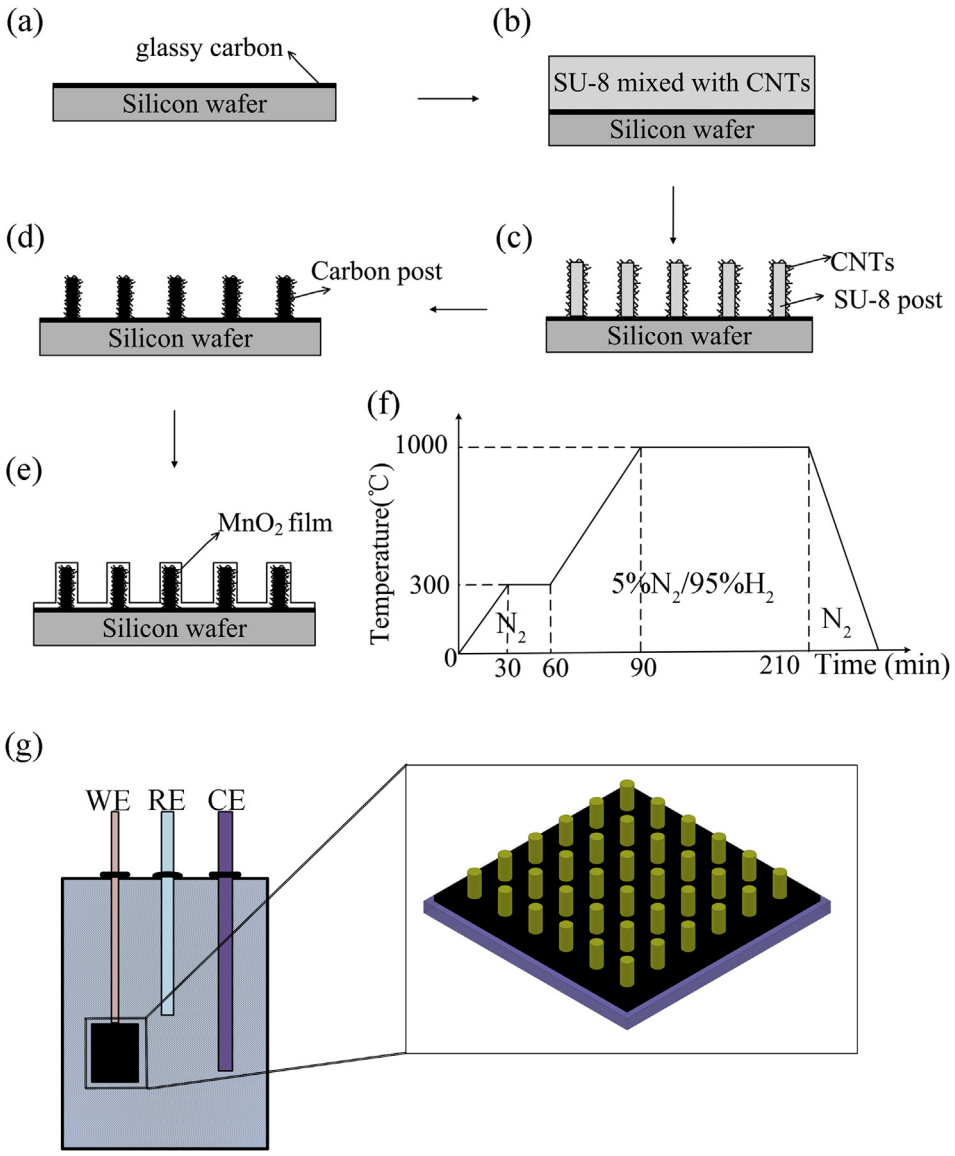

Fig. 1. Typical fabrication process of the microelectrodes. (a) Fabricating the carbon film; (b) spin-coating of CNT-dispersed-photoresist; (c) photolithography; (d) pyrolysis; (e) electrochemical deposition; (f) temperature control curve during the pyrolysis step of (d); (g) schematic view of the three-electrode system. Inset is 3D view of the structure.

specific capacitance of 1370 F g^{-1} [14], low-cost, environmental friendliness, and abundant resources [20].

In addition, improving the design of device architectures is also an effective way to enhance the capacitive performances of on-chip microcapacitors [6,8,15,21–24]. Chen et al. [23] designed 3D structure for micro-supercapacitor using deep reactive ion etching (DRIE) technology. Kang et al. [21] proposed an asymmetric MnO_2–carbon micro-supercapacitor by inductively-coupled plasma etching technology. Wang et al. [6,15,24] reported the fabrication of 3D microelectrodes for micro-supercapacitor through Carbon-MEMS technology and this method was proved to be simple and efficient. Compared with conventional thin film electrodes, 3D microelectrodes with high effective surface area have drawn increasing attention, because they are capable of on-chip integration and have excellent capacitive performance [22]. Although many groups have been engaged in improving the electrochemical performance of microcapacitors, current research on micrometer-sized 3D electrodes with large specific capacitance and good cycling performance is rather limited [22,23]. Therefore, low-cost and large-scale production approaches for on-chip integrated high-performance microelectrodes are in urgent need.

Recently, our group introduced a facile approach to fabricate CNT-integrated carbon microelectrodes by photolithography of CNTs modified SU-8 photoresist and pyrolysis [25]. The 3D carbon structures showed great potential for on-chip electrochemical applications. In this study, we have developed an approach to fabricate large-scale hybrid 3D microelectrodes by electrodeposition of MnO_2 film onto the surface of CNT-integrated carbon microelectrodes, and the electrochemical performance of the hybrid microelectrodes was evaluated for on-chip microcapacitors.

2. Experimental

2.1. Fabrication of 3D hybrid microelectrodes

A typical process to fabricate hybrid 3D microelectrodes is shown in Fig. 1, which mainly consists of spin-coating, photolithography, pyrolysis, and electrochemical deposition. Firstly, the cleaned wafer

(phosphorus doped n-type silicon <100> wafer with a resistivity of 0.01–0.02 cm) was spin-coated with a positive photoresist AZ5214 (AZ Electronic materials) at 500 revolutions per minute (rpm) for 10 s and 3000 rpm for 40 s, then the photoresist was baked at 95 °C for 3 min. A thin film of carbon was obtained by a pyrolysis process at 600 °C (heating rate of 5 °C min^{-1}) for 60 min in 5% H_2/95% N_2 atmosphere environment, which was designed as electric connection and current collector as shown in Fig. 1a. In the next step, photolithography process as shown in Fig. 1b and c was conducted to fabricate CNT-integrated SU-8 posts, and the details were reported previously [25,26]. In this work, the photolithography process was further improved. 20 mg of single-walled carbon nanotubes (SWNTs, 1/3 metallic and 2/3 semiconducting SWNTs, from Chengdu Organic Chemical Co., Ltd) were mixed in 10 ml Monomethyl Ether Acetate (PGMEA, SU-8 diluents from Micro Chem, USA) followed by sufficient ultrasonication in water bath at about 30 °C to form uniform slurry. After that, the uniform slurry was mixed in 40 ml SU-8 photoresist (GM 1070 from Gersteltec Sarl, Switzerland) and ultrasonicated for about 2 h. Thereafter, the CNT-mixed-photoresist was obtained. Similarly, CNT-mixed-developer suspension was prepared by adding 30 mg of SWNTs into 50 ml of PGMEA followed by ultrasonication for 4 h in water bath at 30 °C. The CNTs in the developer suspension were integrated onto the SU-8 posts through self-assembly effect of the nanostructures. And the good adhesion between CNTs and polymer-derived carbon electrodes can be ensured by the homogenous texture of the integrated structure. The CNT-dispersed-photoresist was spin-coated on the as-fabricated carbon film at 500 rpm for 10 s and 1000 rpm for 30 s. After a soft bake at 65 °C for 15 min and 95 °C for 1 h, exposure was carried out in a Karl Suss MA6 contact aligner. The post bake process was carried out at 95 °C for 40 min. After 10 min delay time, development was performed using the as-obtained developer for about 6 min. The 3D carbon microelectrode arrays were obtained by carbonizing the CNT-integrated SU-8 posts using a furnace (GSL-1400X), as shown in Fig. 1d. The heating temperature curve is shown in Fig. 1f, where the heating rate is controlled to be 10 °C min^{-1} with the maximum temperature of 1000 °C.

An electrochemical deposition technique was performed to deposit MnO_2 film on the as-fabricated carbon microelectrode arrays, as shown in Fig. 1e. The process was conducted under galvanostatic conditions at the constant current density of 1 mA cm^{-2} by an electrochemical workstation Autolab PGSTAT302N (Metrohm AG). The manganese sulfate ($MnSO_4.H_2O$) and sodium sulfate (Na_2SO_4) were provided by Sinopharm Chemical Reagent Co., Ltd, and used as received without any further purification. The solution with 0.1 M $MnSO_4$ and 0.1 M Na_2SO_4 was used as electrolyte for electrodeposition of MnO_2 [27]. The as-prepared CNTs-integrated carbon microelectrode arrays were used as working electrode (WE) as shown in Fig. 1g. A platinum wire was used as counter electrode (CE), and Ag/AgCl was used as reference electrode (RE). By varying the deposition time from 5 min to 20 min, different morphologies of MnO_2 films were obtained. After deposition, these samples were washed with distilled water to eliminate any loosely attached chemical substance and dried naturally. Then the 3D carbon microelectrode arrays integrated with CNTs and thin MnO_2 film were fabricated. The overall process is scalable.

2.2. Characterization

Structural properties and electrochemical performance of the as-fabricated samples were investigated in this study. The morphologies of carbon microelectrode arrays and MnO_2 films were characterized by scanning electron microscopy (SEM, Sirion 200) equipped with energy-dispersive x-ray (EDX). The oxidation state of Mn was characterized by X-ray Photoelectron Spectroscopy (XPS, VG Multilab 2000). The cyclic voltammetry (CV) and electrochemical impedance spectroscopy (EIS) tests were carried out via the electrochemical workstation (Autolab PGSTAT302N). The CV test was carried out at the voltage range of −0.1 V to 0.9 V and at different sweep rates ranging from 5 mV s^{-1}–100 mV s^{-1}. Galvanostatic charging/discharging test was conducted using a battery tester (LAND-CT2001A) with the voltage window of −0.1 V to 0.9 V at various current densities from 0.5 mA cm^{-2}–3 mA cm^{-2}. All the electrochemical experiments were carried out in 1 M Na_2SO_4 electrolyte using a three-electrode cell at room temperature, as shown in Fig. 1g.

3. Results and discussions

3.1. Structural characterizations

Fig. 2a shows typical SEM images of the CNT-integrated SU-8 photoresist post array. The diameter of the SU-8 photoresist posts is around 20 μm. The SEM image of single SU-8 post is shown in Fig. 2b with the enlarged view of CNTs on the surface of the post, and the coverage of CNTs is accomplished through self-assembly effect during development process.

After carbonization and electrochemical deposition, typical SEM images of the as-fabricated microelectrodes at different deposition time of MnO_2 are shown in Fig. 3. Fig. 3a–c shows the single post after electrochemical deposition of MnO_2 for 5 min, 10 min and 20 min respectively, while higher magnification SEM images of the corresponding surface morphology of MnO_2 film are presented in Fig. 3d–f respectively. With the relative short electrochemical deposition time such as 5 min, the 3D carbon microelectrode surface is covered mostly by the MnO_2 particle islands (Fig. 3a and d). When the deposition duration is prolonged, the MnO_2 particle islands on the surface of the microelectrode array evolve into more compact film (Fig. 3b and e). With the deposition time of 20 min, the surface is fully covered by the dense film as shown in Fig. 3c and f. In addition, with the increase of deposition time, the diameters of the posts are becoming larger and larger due to the increase of the deposited film thickness. As shown in Fig. 3a–c, the post diameter is estimated to be 11 μm, 12.3 μm, and 14.6 μm respectively. To subtract the carbon post diameter of around 10 μm before electrochemical deposition, the corresponding thickness of the deposited film is estimated to be 0.5 μm, 1.15 μm, and 2.3 μm for 5 min, 10 min and 20 min deposition respectively.

Generally, the formation of MnO_2 on the 3D carbon electrode surface occurs according to the following reactions [28].

$$Mn^{2+} + 2H_2O \rightarrow Mn^{(3+\Delta)} + (1+\Delta)e^- \rightarrow MnO_2 + 4H^+ + 2e^- \quad (1)$$

In brief, Mn(II) ions are firstly oxidized to the thermodynamically unstable intermediate species of Mn(III) ions. Then MnO_2 is chemically formed by disproportionation reaction of Mn(III) ions before Mn(III) ions are reduced to yield Mn(II) ions [29]. Fig. 4a shows the overall structure of the microelectrode array with 10 min deposition of MnO_2 film. The EDX analysis of the film is shown in Fig. 4b, showing that three elements of C, Mn and O exist in the film. A surface elements analysis was also carried out for the deposited film using XPS. The obtained spectrum (Fig. 4c) consists of two main peaks with the Mn $2p_{3/2}$ at a binding energy of 642.1 eV and the Mn $2p_{1/2}$ at 653.7 eV. These peak values indicate the sole existence of Mn^{4+}, i.e., the oxide nanocrystals are MnO_2, which is also in agreement with those reported for MnO_2 [30].

3.2. Capacitance of the microelectrodes

Studies for respective effects of CNTs and MnO_2 film on the CV performance of the hybrid microelectrodes were conducted, and

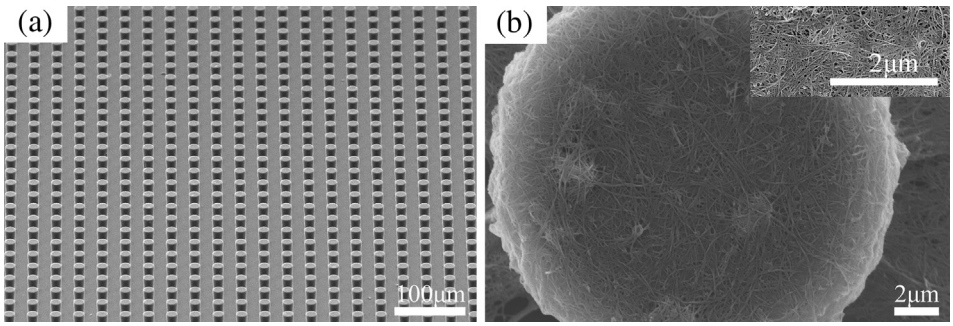

Fig. 2. (a) Typical SEM image of the CNTs integrated SU-8 posts; (b) SEM image of single SU-8 post in (a),with the enlarged SEM image of CNTs as an inset.

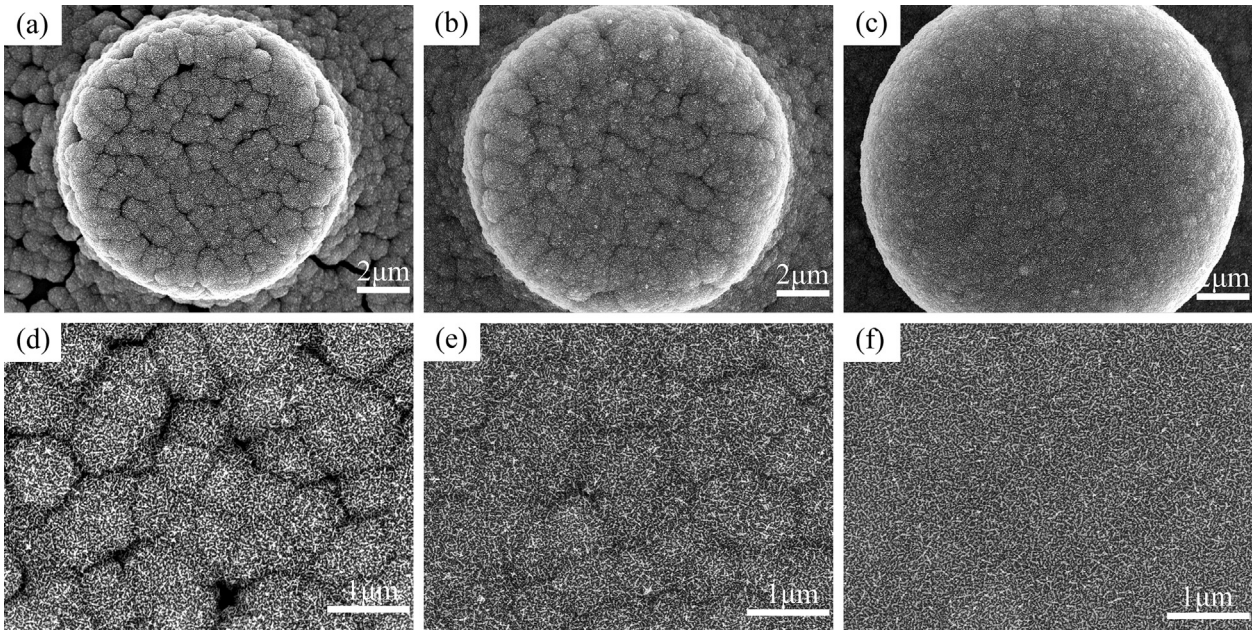

Fig. 3. SEM images of microelectrodes with different MnO_2 deposition time. (a) 5 min; (b) 10 min; (c) 20 min; (d) enlarged SEM image of the post in (a); (e) enlarged SEM image of the post in (b); (f) enlarged SEM image of the post in (c).

the effects of MnO_2 deposition duration on the microelectrodes were also investigated. As shown in Fig. 5a, the voltammetric current can be significantly increased via the stacking of MnO_2 film on the carbon microelectrode, while CNTs integrated in the carbon microelectrode increase the voltammetric current to some extent. The hybrid microelectrode integrated with both MnO_2 film and CNTs has the largest voltammetric current, indicating the best capacitive performance. It suggests that the synergistic effects of CNTs and MnO_2 film contribute to the voltammetric current increment of the composite structure [31]. It is also in agreement with the literature that CNTs can increase the conductivity and surface area of the carbon posts, while the MnO_2 film is able to greatly enhance the capacitance. For carbon materials, the capacitances arise from the pure electrostatic charge accumulated at the interface of electrolytes and the charged electrodes. The pseudocapacitance of MnO_2 film is mainly contributed by the surface

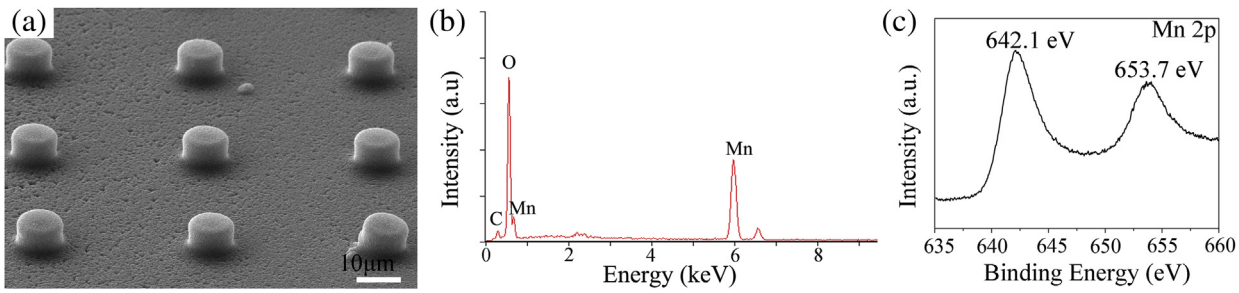

Fig. 4. (a)The microelectrode array with 10 min deposition of MnO_2 film; (b) the EDX analysis of MnO_2 film; (c) XPS pattern of the MnO_2 film.

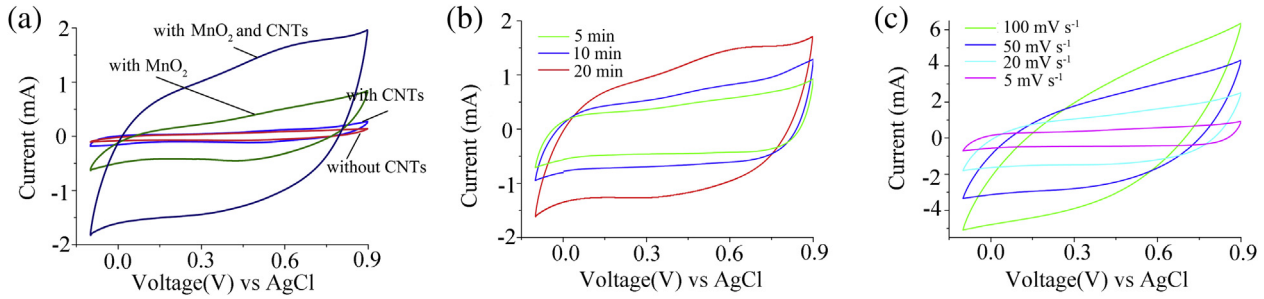

Fig. 5. (a) CV curves of different microelectrodes at the scan rate of 5 mV s^{-1} in 1 M Na_2SO_4 electrolyte; (b) CV curves of the microelectrodes with different MnO_2 deposition time at the scan rate of 5 mV s^{-1} in 1 M Na_2SO_4 electrolyte; (c) CV curves of the sample with 5 min MnO_2 deposition at different scan rates.

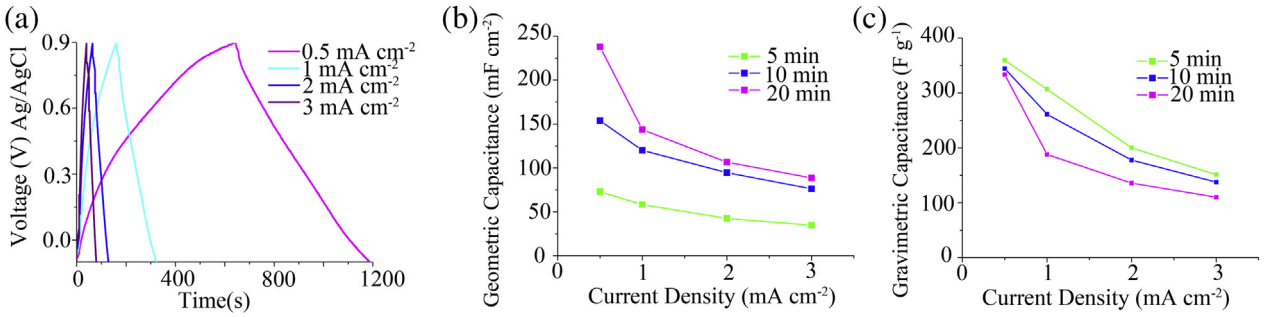

Fig. 6. (a) Galvanostatic charging/discharging curves of the sample with 20 min deposition of MnO_2 at different current densities. (b) Specific geometric capacitances of the microelectrodes with different MnO_2 deposition time at various current densities. (c) Specific gravimetric capacitance of the microelectrodes with different MnO_2 deposition time at various current densities.

faradic reaction and bulk faradic reaction, which occur on the surface and in the bulk of MnO_2 film in contact with the aqueous Na_2SO_4 electrolyte according to the following reactions [32].

$$(MnO_2)_{surface} + Na^+ + e^- \leftrightarrow \left(MnO_2^- Na^+\right)_{surface} \quad (2)$$

$$(MnO_2)_{bulk} + Na^+ + e^- \leftrightarrow (MnOONa)_{bulk} \quad (3)$$

To investigate the influence of surface morphology and thickness of MnO_2 on the electrodes' capacitance, the microelectrodes with different deposition durations were tested. Representative CV curves of the microelectrodes are shown in Fig. 5b with MnO_2 deposition of 5 min, 10 min and 20 min at the scan rate of 5 mV s^{-1} in 1 M Na_2SO_4 electrolyte. The CV curves show a near symmetric rectangular shape and exhibit near mirror-image current response on voltage reversal, which indicates that these structures have good capacitive behavior. When deposited for 20 min, the CV curves exhibit higher capacitive current because there are more substances actively participating in the faradic reaction. The CV curves of the electrodes with 5 min deposition at different scan rates are shown in Fig. 5c. It is obvious that CV curves of the electrode are close to rectangle at lower scan rates of 5 mV s^{-1} and 20 mV s^{-1}, but deform seriously when the scan rate increases. The deformation can be attributed to the kinetically limited pseudocapacitive reactions mentioned earlier and diffusion limited charge transport in the MnO_2 film [21].

To further evaluate the electrochemical properties of the as-fabricated microelectrodes, the galvanostatic charging/discharging measurement was carried out. The charging/discharging performance is shown in Fig. 6a at the current densities from 0.5 mA cm^{-2}–3 mA cm^{-2}. The charge curves are relatively symmetric to the corresponding discharge curves, which indicates good electrochemical behavior of the microelectrode. The discharge curves are approximately straight lines after the initial drop. The rapid change in voltage at the beginning of each charging/discharging half cycle is shown in Fig. 6a. This phenomenon is commonly named IR drop and indicative of equivalent series resistance (ESR), which is related to ionic resistance of electrolyte, intrinsic resistance of the hybrid microelectrode, and interfacial contact resistance between the hybrid electrode and electrolyte [19]. The value of ESR is obtained through dividing the voltage drop by twice of the current [33], from the IR drop in charging/discharging curve in Fig. 6a, which is about 7.5 Ω at the current density of 0.5 mA cm^{-2}. Moreover, the capacitance can be calculated through the linear parts of discharge curves according to the following formula [34]:

$$C = \frac{I_A \times \Delta t}{\Delta V} \quad (4)$$

where I_A (mA) is the current for charge–discharge, Δt (s) is the discharging time. ΔV can be calculated from approximately the middle value of the voltage range to maximum voltage for the calculation [33]. The specific geometric and gravimetric capacitance of the microelectrodes can be calculated through Equations (5) and (6), respectively.

$$C_A = \frac{I_A \times \Delta t}{\Delta V \times A} \quad (5)$$

$$C_m = \frac{I_A \times (\Delta t_{C@MnO_2} - \Delta t_C)}{\Delta V \times m_{MnO_2}} \quad (6)$$

where A (cm^2) is the electrode projected area, and m_{MnO_2} is the mass of MnO_2 film, which is calculated by the following Equation (7) assuming 100% current efficiency via reaction (1) and Faraday's law [35].

$$m_{MnO_2} = \frac{Q \times M}{2 \times e \times N_A} \quad (7)$$

where Q is the charge passed through the deposition reaction, M is the molecular mass of MnO_2 (86.94 g mol^{-1}), e is electron charge, and N_A is Avogadro's number. As shown in Fig. 6b, the specific geometric capacitance of the microelectrode deposited for 20 min is higher than that of microelectrodes with shorter deposition durations for all current densities. For example, at the current density of 0.5 mA cm^{-2}, the specific geometric capacitance of the microelectrode is about 73 mF cm^{-2} with 5 min MnO_2 deposition, while the specific geometric capacitance is about 238 mF cm^{-2} when the deposition time is 20 min. This is because there are more substances actively participate in the faradic reaction when the microelectrode is fabricated with prolonged deposition time. Even though the electrochemical performance in this study is not as good as the results reported previously [36], in which the specific geometric capacitance of the MnO_2–CNT composite electrode reaches 470 mF cm^{-2}, our approach has the advantage of applying this facile method for mass fabrication of on-chip microcapacitor electrodes. The specific gravimetric capacitance decreases gradually with the increase of deposition time as shown in Fig. 6c. The specific gravimetric capacitance is around 359.4 F g^{-1} for the deposition of 5 min while it is decreased to 333.4 F g^{-1} for 20 min deposition at the current density of 0.5 mA cm^{-2}. The higher specific gravimetric capacitance for shorter deposition duration of MnO_2 film is attributed to the larger surface area of MnO_2 film as shown in Fig. 3, which facilitates higher utilization efficiency of the active materials in the microelectrode. Generally, the mass of active MnO_2 will increase with the prolonging of deposition time, but too much loading of MnO_2 might lower the conductivity of the composite electrodes and limit the electrochemical performance of the hybrid microelectrode. We have conducted separate experiments in our work, when the deposition time was prolonged to 25 or 30 min, the electrochemical performance was observed to be not as good as that of shorter deposition time. Additionally, with the increase of current density, both the specific geometric and gravimetric capacitances decrease gradually as shown in Fig. 6b and c. It has been reported that when the current density is low, it is easy for the ions to diffuse into the available pores of the electrode, so the insertion process will be reacted thoroughly and the specific capacitance is large. On the contrary, when the current density is increased, the effective utilization of the electrodes is mainly the outer surface of the MnO_2 film. So the efficient interaction between the electrode and the ions is much reduced [1]. It is also noticed that the capacitance decreases greatly with the increase of current density from 0.5 mA cm^{-2} to 1 mA cm^{-2} for the 20 min deposition over the carbon microelectrode (Fig. 6b and c). Thick MnO_2 with dense nature which depresses the diffusion rate of electrolytes into the matrix should account for the decrease of specific capacitance [36]. At the current density of 1 mA cm^{-2}, the specific capacitance keeps 144 mF cm^{-2}, which is larger than 30 mF cm^{-2} reported by Kang et al. [21]. Even though nanoscopically thin MnO_2 film offers higher gravimetric capacitance and better utilization of the MnO_2 film, and the diffusion distances for the solid-state transport of insertion cations can be reduced, they are substantially unsuitable for practical energy storage (e.g., integrated devices) because of low volumetric capacitance [21,36,37]. Depositing relative thicker MnO_2 film onto the well-ordered microelectrodes is an efficient way to improve the capacitance of on-chip integrated devices [38]. However, too thick film may limit its optimal electrochemical performance as mentioned earlier. Therefore, the control of MnO_2 film thickness and surface morphology is critical to improve the performance of the hybrid microelectrode structure, which can be optimized by the fabrication process.

Nyquist plot of the microelectrode array (1 cm^2) with 20 min deposition of MnO_2 from 0.01 Hz to 10^5 Hz at open circuit potential is shown in Fig. 7, and the EIS data has been fitted by the equivalent circuit model as shown in the inset. In the equivalent circuit model, R1 means the ESR. R2 means charge-transfer resistance. Two constant phase elements CPE1 and CPE2 are used to describe the double layer capacitance at the interface of the electrolyte and the hybrid microelectrode, and the pseudocapacitance from ions transfer in the MnO_2 film, respectively [23]. The value of R1 is 8.4058 Ω, which is in reasonable agreement with the estimates from galvanostatic charge/discharge measurements. The thick and dense MnO_2 film (~2.3 μm) leads to the increase in ESR due to the poor conductivity of MnO_2 [36]. The presence of semicircle in the high frequency range corresponds to R2, and is associated with the surface property of the hybrid microelectrode. The large R2 (54.5 Ω) inhibits the Na^+ insertion/adsorption process in MnO_2, leading to low rate capability of the hybrid microelectrode as shown in Fig. 6b and c [32].

Cycling performance is also important for on-chip supercapacitors. The cycling test of the 3D carbon microelectrode array with 20 min deposition of MnO_2 was carried out, as shown in Fig. 8. The inset is typical charging/discharging curves at the current density of 1 mA cm^{-2} between −0.1 V and 0.9 V in 1 M Na_2SO_4 electrolyte. The capacitance retains around 81.8% of the original value after 6000 charge–discharge cycles. It is suggested that the structure distortions caused by the weak mechanical adhesion between Si wafer and the carbon structure lead to capacitance

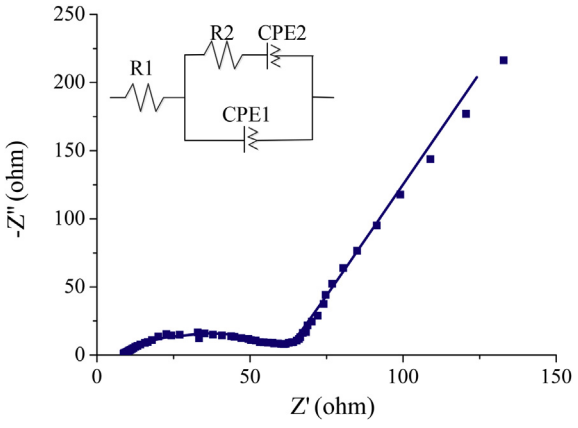

Fig. 7. Nyquist plot of the sample from 0.01 Hz to 100 kHz. Z' is the real impedance and Z'' is the imaginary impedance with the equivalent circuit model as an inset.

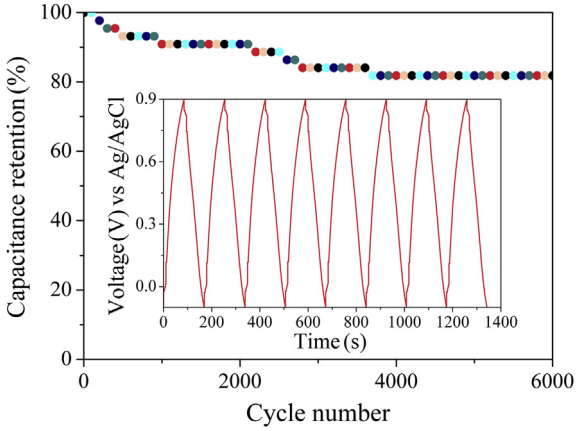

Fig. 8. Cyclic performance and capacitance retention for the sample with 20 min deposition of MnO_2 with typical charging/discharging curves at the current density of 1 mA cm^{-2} as an inset.

fading upon cycling, which needs to be further explored to improve the structure reliability. Furthermore, as mentioned earlier, the charge storage mechanism between carbon material and MnO_2 film is different. The difference will lead to a certain degree of volume change in the as-fabricated hybrid microelectrode during cycling. This change was reported to cause mechanical failure of the hybrid microelectrode which will also result in capacitance fading [22,39]. The result is better than that of the symmetric polypyrrole/Carbon-MEMS micro-supercapacitor [22], which retains only 56% of its initial capacitance after 6000 cycles. Moreover, the proposed fabrication process can be further optimized to improve the electrochemical performance of the hybrid microelectrode structure. In general, the integration of MnO_2 film and CNTs to Carbon-MEMS microelectrodes offers a promising large-scale manufacturing approach for high-performance on-chip microcapacitors.

4. Conclusion

A hybrid structure of 3D carbon microelectrode array integrated with CNTs and MnO_2 film is presented for on-chip microcapacitors, and the fabricating process based on carbon-MEMS is simple and scalable for large-scale production. With the introduction of CNTs and MnO_2 film, the electrochemical performance of the 3D microelectrodes has been improved significantly. The specific geometric capacitance achieves up to 238 mF cm^{-2} at the current density of 0.5 mA cm^{-2} with the deposition of MnO_2 film. And the capacitance retention is about 81.8% after 6000 cycles. It is concluded that the high-performance 3D hybrid microelectrodes have promising applications in on-chip microcapacitors.

Acknowledgments

This work is supported by National Science Foundation of China (No. 51275195 and 91323106) and 973 program (No. 2009CB724204). We would like to thank the Analytical and Testing Center of Huazhong University of Science and Technology for the sample preparation and characterization.

References

[1] H.Z.V. Subramanian, R. Vajtai, P.M. Ajayan, B. Wei, J. Phys. Chem. B 109 (2005) 20207–20214.
[2] M.S. Dresselhaus, I.L. Thomas, Nature 414 (2001) 332–337.
[3] P. Flynn, Meeting the Energy Needs of Future Warriors, The National Academies Press, 2004.
[4] B.E. Conway, Electrochemical Supercapacitors: Scientific Fundamentals and Technological Applications, Kluwer, New York, 1999.
[5] L.L. Zhang, X.S. Zhao, Chem. Soc. Rev. 38 (2009) 2520–2531.
[6] C. Liu, F. Li, L.P. Ma, H.M. Cheng, Adv. Mater. 22 (2010) E28–E62.
[7] A. Burke, J. Power Sources 91 (2000) 37–50.
[8] M. Beidaghi, W. Chen, C. Wang, J. Power Sources 196 (2011) 2403–2409.
[9] J.J. Yoo, K. Balakrishnan, J. Huang, V. Meunier, B.G. Sumpter, A. Srivastava, M. Conway, A.L. Reddy, J. Yu, R. Vajtai, P.M. Ajayan, Nano Lett. 11 (2011) 1423–1427.
[10] Z. Fan, J. Chen, B. Zhang, F. Sun, B. Liu, Y. Kuang, Mater. Res. Bull. 43 (2008) 2085–2091.
[11] B. Kim, H. Chung, W. Kim, Nanotechnology 23 (2012) 155401.
[12] L.I. Hill, A. Verbaere, D. Guyomard, J. Electrochem. Soc. 150 (2003) D135–D148.
[13] S. Devaraj, N. Munichandraiah, J. Phys. Chem. C 112 (2008) 4406–4417.
[14] M. Toupin, T. Brousse, D. Be'langer, Chem. Mater. 16 (2004) 3184–3190.
[15] W. Chen, M. Beidaghi, V. Penmatsa, K. Bechtold, L. Kumari, W.Z. Li, C. Wang, IEEE Trans. Nanotechnol. 9 (2010) 734–740.
[16] B. Sajdl, K. Micka, P. Krtil, Electrochim. Acta 40 (1995) 2005–2011.
[17] C.C. Hu, K.H. Chang, M.C. Lin, Y.T. Wu, Nano Lett. 6 (2006) 2690–2695.
[18] Y.E. Miao, W. Fan, D. Chen, T. Liu, ACS Appl. Mater. Interfaces 5 (2013) 4423–4428.
[19] B. Hsia, M.S. Kim, M. Vincent, C. Carraro, R. Maboudian, Carbon 57 (2013) 395–400.
[20] G. Yu, L. Hu, M. Vosgueritchian, H. Wang, X. Xie, J.R. McDonough, X. Cui, Y. Cui, Z. Bao, Nano Lett. 11 (2011) 2905–2911.
[21] C. Shen, X. Wang, S. Li, J. Wang, W. Zhang, F. Kang, J. Power Sources 234 (2013) 302–309.
[22] M. Beidaghi, C. Wang, Electrochim. Acta 56 (2011) 9508–9514.
[23] W. Sun, R. Zheng, X. Chen, J. Power Sources 195 (2010) 7120–7125.
[24] A.L.M. Reddy, M.M. Shaijumon, S.R. Gowda, P.M. Ajayan, J. Phys. Chem. C 114 (2010) 658–663.
[25] L. Zhang, T. Shi, S. Xi, D. Liu, Z. Tang, X. Li, W. Lai, Thin Solid Films 520 (2011) 1041–1047.
[26] S. Xi, T. Shi, D. Liu, L. Xu, H. Long, W. Lai, Z. Tang, Sens. Actuators A Phys. 198 (2013) 15–20.
[27] H. Xia, J. Feng, H. Wang, M.O. Lai, L. Lu, J. Power Sources 195 (2010) 4410–4413.
[28] G.H.A. Therese, P.V. Kamath, Chem. Mater. 12 (2000) 1195–1204.
[29] A. Manivel, N. Ilayaraja, D. Velayutham, M. Noel, Electrochim. Acta 52 (2007) 7841–7848.
[30] W. Xiao, H. Xia, J.Y.H. Fuh, L. Lu, J. Electrochem. Soc. 156 (2009) A627.
[31] Y. Cheng, S. Lu, H. Zhang, C.V. Varanasi, J. Liu, Nano Lett. 12 (2012) 4206–4211.
[32] W. Wei, X. Cui, W. Chen, D.G. Ivey, J. Phys. Chem. C 112 (2008) 15075–15083.
[33] M.D. Stoller, R.S. Ruoff, Energy Environ. Sci. 3 (2010) 1294–1301.
[34] H. Li, J. Wang, Q. Chu, Z. Wang, F. Zhang, S. Wang, J. Power Sources 190 (2009) 578–586.
[35] J. Duay, E. Gillette, R. Liu, S.B. Lee, Phys. Chem. Chem. Phys. 14 (2012) 3329–3337.
[36] Y.T. Wu, C.C. Hu, J. Electrochem. Soc. 151 (2004) A2060–A2066.
[37] C. Xu, F. Kang, B. Li, H. Du, J. Mater. Res. 25 (2011) 1421–1432.
[38] P. Simon, Y. Gogotsi, Nat. Mater. 7 (2008) 845–854.
[39] H. Jiang, Y. Dai, Y. Hu, W. Chen, C. Li, ACS Sustain. Chem. Eng., http://dx.doi.org/10.1021/sc400313y.